Published February 1, 2019

Original Research

Core Ideas

- A field-scale experiment and numerical simulations confirm salt backfill behavior.
- Simulations closely match temperature around and under the piled salt backfill.
- Results indicate limited dissolution–precipitation reactions around the heat source.
- Alteration of backfill is unlikely if the drift is allowed to dry before emplacement.

Heat-Generating Nuclear Waste in Salt: Field Testing and Simulation

Peter J. Johnson, Shawn Otto, Douglas J. Weaver, Brian Dozier, Terry A. Miller, Amy B. Jordan, Nathan G. Hayes-Rich, and Philip H. Stauffer*

Investigations relating to in-drift disposal of heat-generating nuclear waste in salt have raised questions about heat–brine interactions in the unsaturated run-of-mine (RoM) salt pile used as backfill. These interactions have the potential to change the structure of the RoM salt surrounding the canister, possibly altering long-term containment of the source. An experiment is in progress at the Waste Isolation Pilot Plant (WIPP), New Mexico, in which a heated canister was placed on the floor of an open drift, covered in a pile of RoM salt, and energized with 1000 W. Temperature in the RoM salt pile had stabilized after about 15 d, allowing evaluation of the heat-up period of the ongoing experiment. Using a multiphase porous flow simulator that has been modified to handle salt-specific coupled processes, we examined coupled thermal–hydrological–chemical behavior in the RoM salt pile. Our simulations suggest that for the relatively dry cases examined, porosity changes within RoM salt in a generic salt repository are likely to be minor in the period between waste emplacement and plastic closure of the drift. The primary sensitivity for porosity change is to the early moisture content of the RoM salt used to cover the canister. Secondary influences include moisture availability from the disturbed rock zone (DRZ) surrounding the drift and the capillary pressure ratio between the DRZ and the RoM salt. Early changes in porosity and permeability may be affected by moisture content, but this was not observed in the test. Such changes would be most likely to occur when using damp RoM salt or if waste is emplaced in a drift immediately following opening of the drift before evaporative dewatering of the drift walls occurs.

Abbreviations: HGNW, heat-generating nuclear waste; DRZ, disturbed rock zone; RoM, run-of-mine; WIPP, Waste Isolation Pilot Plant.

P.J. Johnson, T.A. Miller, N.G. Hayes-Rich, and P.H. Stauffer, EES-16: Computational Earth Science, MS T003, Los Alamos National Lab., Los Alamos, NM 87545; S. Otto, D.J. Weaver, and B. Dozier, Los Alamos National Lab. Carlsbad Field Office, Carlsbad, NM 88221; A.B. Jordan, Neptune and Company, Lakewood, CO 80215. P.J. Johnson current address, GNS Science, Wellington, New Zealand. *Corresponding author (stauffer@lanl.gov).

Received 22 Aug. 2018.
Accepted 26 Nov. 2018.

Citation: Johnson, P.J., S. Otto, D.J. Weaver, B. Dozier, T.A. Miller, A.B. Jordan N.G. Hayes-Rich, and P.H. Stauffer. 2019. Heat-generating nuclear waste in salt: Field testing and simulation. Vadose Zone J. 18:180160. doi:10.2136/vzj2018.08.0160

Geologic disposal of high-level heat-generating nuclear waste (HGNW) remains a primary conceptual pathway to ensure the long-term safety and security of disused nuclear materials. Bedded salt has been a material of interest since at least 1957 (Hess et al., 1957) because it has numerous properties that are expected to aid in the containment and isolation of nuclear waste, e.g., viscoplastic closure of fractures, low porosity and permeability, and high thermal conductivity (Hansen and Leigh, 2011). More recently, studies pertaining to nuclear waste disposal in salt have been conducted in Germany (Brewitz and Rothfuchs, 2007; Fahland and Heusermann, 2013; Wollrath et al., 2014) and in the United States at the Waste Isolation Pilot Plant (WIPP; see Rechard, 2000), the location for the present study. A primary goal of ongoing international efforts is to establish the safety case for bedded salt as a potential host material for high-activity HGNW.

One proposed concept for HGNW emplacement in salt is referred to as *in-drift* disposal (Washington Savannah River Company et al., 2008; Carter et al., 2011; Hansen and Leigh, 2011; Robinson et al., 2012). A horizontal tunnel, in context called a *drift*, is carved into the rock salt layer. A canister containing the HGNW is placed on the floor of this drift and covered with crushed salt extracted from the mining process, referred to as run-of-mine (RoM) salt, for shielding. After filling with waste canisters, the drift is backfilled with RoM salt. Viscoplastic closure of any remaining voids in the drift follows naturally (Hess et al., 1957; Rechard, 2000; Hansen and Leigh, 2011) and reduces the potential for migration of radioactive material.

Recent studies pertaining to the in-drift disposal concept identified a need to improve the current understanding of constitutive relationships in both RoM and solid salt to better constrain the long-term safety case for HGNW in any future salt repository (Callahan et al., 2012; Stauffer et al., 2015; Hansen et al., 2017). One important uncertainty related to the in-drift concept concerns heating-induced changes in the RoM salt pile that alter brine and water vapor flow near the canister and could impact the short-term performance through changes to the mechanical properties of the RoM salt backfill (Stauffer et al., 2015). A series of field-scale tests was proposed that aim to examine this and related topics (USDOE Carlsbad Field Office, 2012; Stauffer et al., 2013, 2015; Jordan et al., 2015a, 2015b, 2015c; Bourret et al., 2016; Johnson et al., 2017a). An operational test of one of these experiments is currently underway. This experiment features a stainless steel canister containing a heater assembly, representing a mock-up of a HGNW canister.

Data from the operational test can be used to examine the changes in the RoM salt resulting from multiphase flow interactions (Faghri, 1995; Olivella et al., 2011; Jordan et al., 2015a) within the salt pile. Evaporation of brine near the heat source triggers precipitation of salt and the closure of porosity and reduction of permeability, while condensation of moisture in cooler areas leads to the dissolution of salt and increases in porosity and permeability (Jordan et al., 2015a; Olivella et al., 2011; Blanco-Martín et al., 2018). Dissolution–precipitation reactions resulting from evaporation and condensation of brine (Olivella et al., 2011; Bourret et al., 2017; Johnson et al., 2018) may strongly affect fluid flow to and around the waste canister. Based on this conceptual model and prior experimental work, heat–brine–vapor–salt interactions near the canister are hypothesized to result in one of two outcomes: (i) evaporation of brine near the canister and the creation of a dry halo around the heat source, with inadequate brine recharge to the heater to cause strong porosity and permeability effects (Hansen and Leigh, 2011), or (ii) brine recharge to the heat source, porosity and permeability changes throughout the RoM salt pile, and potential impacts on the canister (Stauffer et al., 2013; Bourret et al., 2017; Johnson et al., 2017b). Multiphase flow and material changes in repository salt are complex and are being explored through a variety of approaches, including coupling of thermal, hydrological, mechanical, and chemical processes (Birkholzer, 2004; Caporuscio et al., 2013; Kuhlman and Malama, 2013; Bourret et al., 2016; Rutqvist et al., 2016; Johnson et al., 2017b). This work focuses on the impacts of coupling thermal convection, multiphase liquid and vapor flow, and chemical precipitation–dissolution reactions.

Here we report results from simulations of an in-progress heated canister experiment at WIPP using the Los Alamos National Laboratory porous flow simulator FEHM (Finite Element Heat and Mass; https://fehmn.lanl.gov; Zyvoloski et al., 2012). FEHM has been recently modified to include salt-specific reactions (Stauffer et al., 2013; Jordan et al., 2015a, 2015b, 2015c; Bourret et al., 2016; Johnson et al., 2018). First, we provide an independent estimate of porosity in the RoM salt pile and calibrate our numerical simulation of the first 15 d of heating based on early temperature results. We then present simulations exploring sensitivity of the system to changes in porosity during 100 d of heating. These simulations are designed to illuminate the relative importance of poorly constrained parameters including (i) the initial saturation of the RoM salt, (ii) the saturation of the disturbed rock zone (DRZ), (iii) the capillary pressure ratio between the DRZ and the RoM salt, and (iv) the elapsed time between opening of the drift and placement of the waste package. Finally, the results are discussed with respect to planning and implementation at possible future high-level-waste repositories in bedded salt formations. Our work aims to improve understanding of the processes that may occur in the shielding surrounding waste during an initial period beginning with drift excavation and waste emplacement prior to the long-term closure and isolation of the drift.

Experimental Design

The experiment features a stainless steel cylindrical canister with internal heating elements (Fig. 1) placed on the floor of a 2.44-m (8-ft) tall drift in bedded salt. This canister is a mock-up of a standard Savannah River HGNW canister and is designed to operate in the hostile WIPP environment. High temperatures, saline brine, and acid gas generation all can cause corrosion of

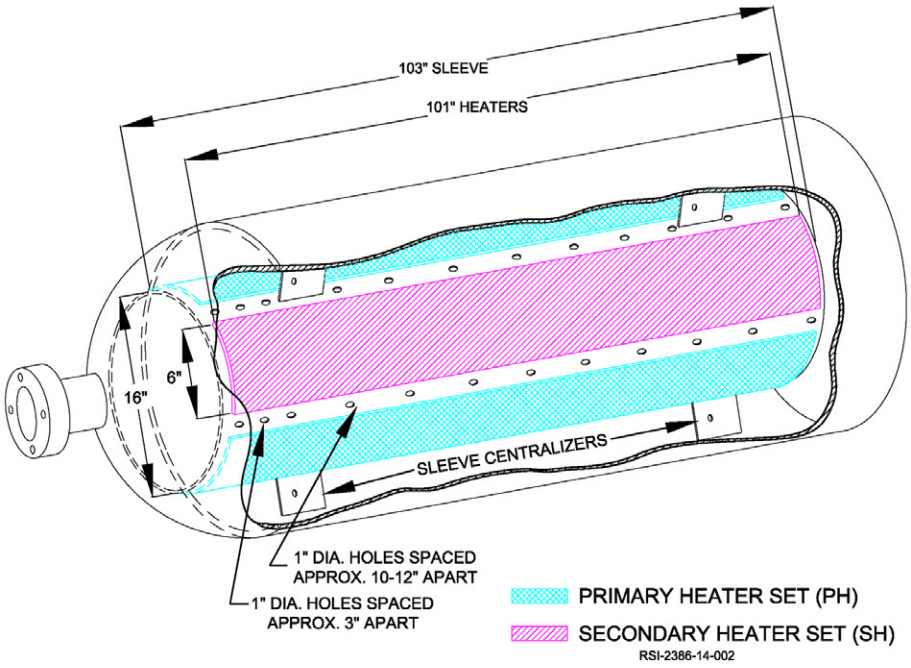

Fig. 1. Schematic of the heater assembly, provided by RESPEC Mining and Energy (Weaver, 2014).

equipment. An assembly inside the canister contains six strip heaters, each capable of outputting 600 W. Three of these heaters are designed to operate as a primary array, with the other three included as a secondary backup array. The heater canister is 2.67 m (8.75 ft) long with a radius of 0.3048 m (1 ft) and is oriented with its long axis in the north–south direction. The interior of the canister is filled with ceramic, spherical sand (cerabeads), which is intended to represent the thermal properties of vitrified nuclear waste (Jordan et al., 2015c). A total of 1000 W is delivered electrically to the three heating elements located inside the canister. A programmable control system limits energy input at the heaters to the desired level. Heater strips are affixed to an inner sleeve assembly inserted inside the canister with centralizing spacers.

The active heaters in the ongoing experiment are the primary array, monitored by thermocouples THEA01, THEA02, and THEA03 in Fig. 2. In the event of failure of these heaters, the secondary set could be activated. Testing of the heater was conducted in a separate set of experiments in 2014 (Jordan et al., 2015c). Figure 3 shows the outside appearance of the final canister setup as placed on the floor of WIPP.

The experiment is located in a horizontal shaft, the drift, near a major entrance into WIPP that is tens of meters long and wide enough for vehicles to pass. Crushed RoM salt covers the canister and forms an asymmetric, flat-topped pile with downward sloping sides (Fig. 4A). The top of the pile is 0.9 m (3 ft) above the center of the canister and 1.2 m (4 ft) above the floor of the drift. Thermocouple arrays are placed extending one canister-radius (0.30 m) vertically (+z direction) and laterally ($\pm x$ direction), with 5.08-cm (2-inch) spacing between measurement points. An additional thermocouple array is placed in a small-diameter borehole beneath the canister and extends to 0.61 m (2 ft) beneath the canister. Based on these measurements, a mesh was constructed for numerical simulations (Fig. 4B).

The walls of the drift consist of intact, bedded salt. The WIPP salt is well characterized in general but shows localized heterogeneities, including small veins of clay, polyhalite, gypsum, fluid inclusions, fractures, and lithologic variability common in bedded evaporites (Powers et al., 1978; Krieg, 1984; Lappin, 1988). A disturbed rock zone (DRZ), also referred to as an excavation damage zone (Tsang et al., 2005), extends into the wall from the open air of the drift. Fracture permeability and a small amount of additional porosity are formed in this region due to pressure unloading caused by deviatory stress concentration and dilatancy of the rock salt and vibrational damage from the mining process. Additional permeability in the DRZ may allow brine from the walls (McTigue and Nowak, 1987) of the drift to enter the RoM salt pile.

Experimental Results

The experiment was activated at 1615 h UTC on 21 Sept. 2017. Approximately steady-state temperatures were attained after 15 d (Fig. 5A). A brief power outage before 20 d can be seen as a drop in temperature in Fig. 5A. Similar temperature values and gradients above and lateral to the heater suggest a conduction-dominated system (Fig. 5B).

Based on the thermal data from the experiment (Fig. 5), an analytical solution for estimating the thermal conduction properties of the RoM salt pile can be developed assuming conductive heat transfer radial to a heated pipe:

$$\kappa = \frac{Q\ln\left(r_2/r_1\right)}{2\pi L\left(\Delta T\right)} \quad [1]$$

where κ is the thermal conductivity (W m^{-1} K^{-1}), Q is the heat input into the relevant canister length (75 W for a 0.2-m-long canister segment), r_2 and r_1 are the locations of the measurements radially from the center of the ring (0.6096 and 0.3048 m, respectively), L is the length of the canister segment (0.2 m), and ΔT is the difference in temperature between the two measurement points. Using an approximated temperature difference of 40°C from the canister

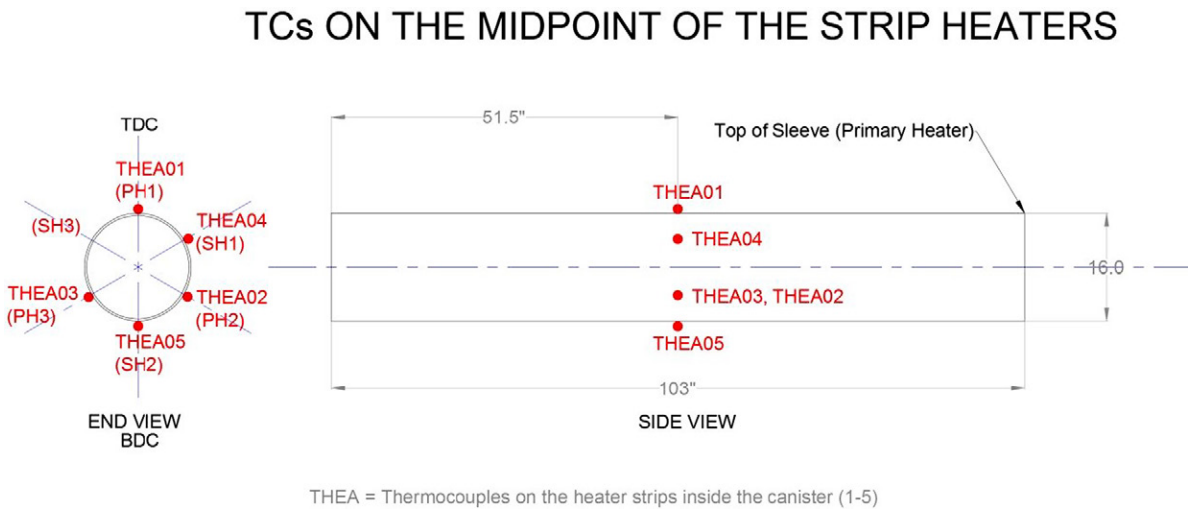

Fig. 2. End view (left) and side view (right) of the heater assembly, showing the locations of heater strips on the canister. Note that the heaters extend most of the length of the canister in the side view. Active heaters for the experiment are THEA01, 02, and 03; TC = thermocouple.

Fig. 3. External view of the complete canister assembly, placed on the drift floor of the Waste Isolation Pilot Plant prior to the addition of the run-of-mine salt pile.

wall (100°C) to the 30.48-cm point (60°C) yields a thermal conductivity of about 1 W m^{-1} K^{-1}. Based on experiments at the Asse salt mine in Germany (Becthold et al., 2004), the thermal conductivity of granular salt scales with porosity (Gable et al., 2009) as

$$\kappa_{\text{T-ASSE}}(n) = -270n^4 + 370n^3 - 136n^2 + 1.5n + 5 \quad [2]$$

This function is valid only for porosities up to about 0.4 but provides a match to the calculated thermal conductivity at a porosity of about 0.3.

Numerical Model Formulation

Simulations of the salt domain are performed using the FEHM code (Zyvoloski et al., 2012). For the present problem, model functions and formulations to handle the chemistry of brine and salt and the effects of salt on the heat and mass transport are used (Stauffer et al., 2015; Johnson et al., 2018). FEHM applies equations for conservation of water mass m, air mass η, and energy e between connected volume elements as

$$\frac{\partial A_m}{\partial t} + \nabla \cdot \mathbf{f}_m + q_m = 0 \quad [3]$$

$$\frac{\partial A_\eta}{\partial t} + \nabla \cdot \mathbf{f}_\eta + q_\eta = 0 \quad [4]$$

$$\frac{\partial A_e}{\partial t} + \nabla \cdot \mathbf{f}_e + q_e = 0 \quad [5]$$

where A is the quantity (mass or energy), $\mathbf{f}$ is the flux of either mass or energy, q is the source–sink term, and t is time. Water mass per unit volume, A_m, is given by

$$A_m = n[S_v\rho_v(1-\eta_v) + S_l\rho_l(1-\eta_l)] \quad [6]$$

and air mass per unit volume, A_η, is

$$A_\eta = n(S_v\rho_v\eta_v + S_l\rho_l\eta_l) \quad [7]$$

where S is the saturation, ρ is the density of the vapor phase and liquid phase (subscripts v and l), n is porosity, and η_v and η_l are the mass fractions of air contained in the vapor and liquid phases, respectively.

Mass fluxes for water and air are

$$\mathbf{f}_m = (1-\eta_v)\rho_v\mathbf{u}_v + (1-\eta_l)\rho_l\mathbf{u}_l \quad [8]$$

and

$$\mathbf{f}_\eta = n(\eta_v\rho_v\mathbf{u}_v + S_l\rho_l\mathbf{u}_l) \quad [9]$$

where $\mathbf{u}$ is the volumetric flux. Darcy's law controls the volumetric flux of the vapor and liquid:

$$\mathbf{u}_v = -\frac{k_{rv}}{\mu_v}(\nabla P_v - \rho_v\mathbf{g}) \quad [10]$$

and

$$\mathbf{u}_l = -\frac{k_{rl}}{\mu_l}(\nabla P_l - \rho_l\mathbf{g}) \quad [11]$$

where k_r is the relative permeability of the respective phases, P is pressure, and $\mathbf{g}$ is the gravitational vector. Relative permeability in the present simulations is a linear fit of saturation. The linear formulation allows numerical stability in the complex coupled thermal–hydraulic–mechanical–chemical salt domains and allows calculation of relative permeability values across the full range of porosities that may occur during simulations. We are working on implementing a faster algorithm using more complex models such as the van Genuchten and Brooks–Corey approaches but note that such functions must be applicable for the full range of porosity values achievable in salt systems. Fluid density and viscosity are polynomial functions of pressure and temperature based on National Bureau of Standards data (Haar et al., 1984).

Energy per unit volume A_e is given as

$$A_e = (1-n)\rho_r\gamma_r + n(S_v\rho_v\gamma_v + S_l\rho_l\gamma_l) \quad [12]$$

with $\gamma_r = C_{pr}T$, and the energy flux $\mathbf{f}_e$ given by

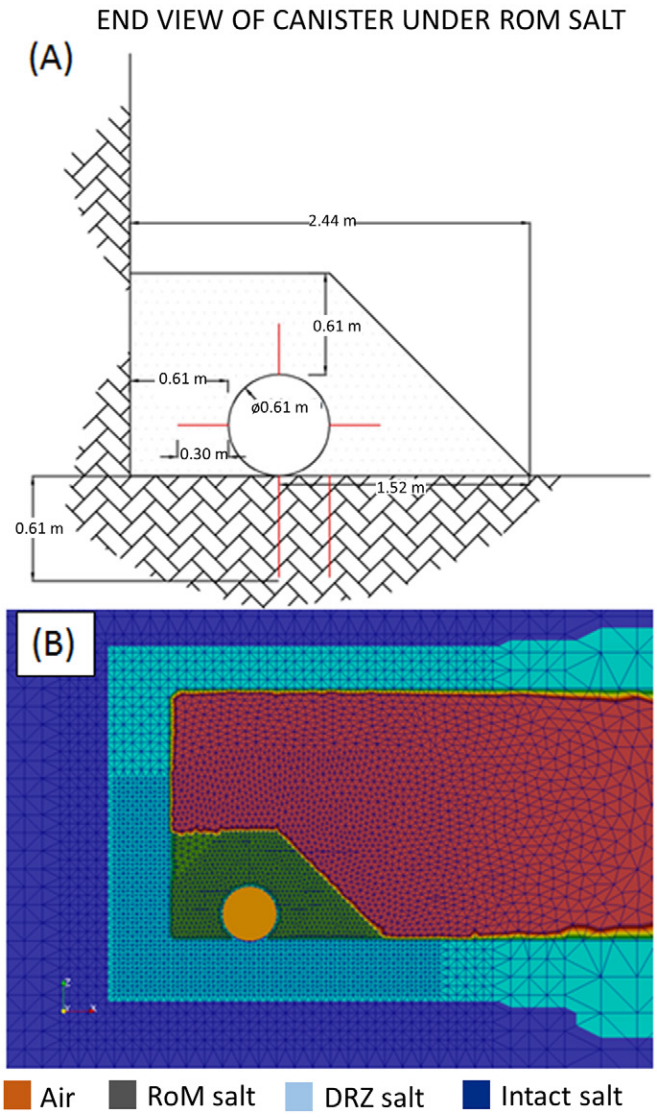

Fig. 4. (A) End view schematic of the canister in the run-of-mine (RoM) salt pile, looking north along the centerline of the canister. Red lines indicate thermocouple arrays. The top and right-hand sides of the pile are surrounded by air. Below and left of the pile is the damaged rock zone (DRZ). (B) 2D mesh and end view of the 3D mesh generated for numerical modeling. Red color indicates air; green is run-of-mine (RoM) salt; light blue is DRZ salt; dark blue is intact rock; the canister is shown with an orange circle. The *y* axis corresponds with the north–south direction; the *x* axis corresponds with the east–west direction; west is to the left.

$$\mathbf{f}_e = \rho_v h_v \mathbf{u}_v + \rho_l h_l \mathbf{u}_l - \kappa \nabla T \quad [13]$$

The subscript *r* refers to the solid phase; γ is the specific internal energy, C_{pr} is the specific heat of the rock, h_v and h_l are specific enthalpies for the vapor and liquid phases, κ is thermal conductivity, and T is temperature. Gravitational potential energy is embedded in the liquid-phase specific enthalpy (or methalpy) definition (Stauffer et al., 2014) in FEHM when gravity is enabled as

$$h_l = C_p T + P_l V_l + gz \quad [14]$$

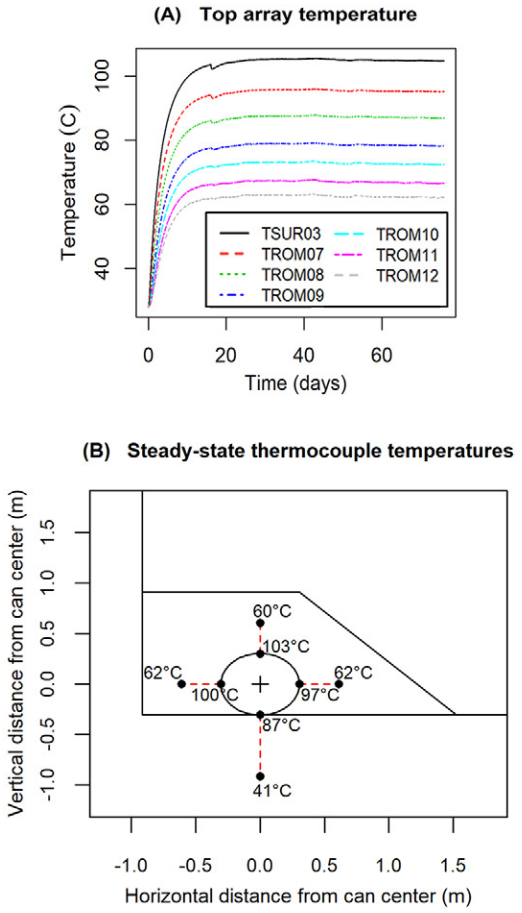

Fig. 5. (A) Temperature of each point of thermocouple array in transect extending vertically upward from canister center (TSUR03 is the thermocouple at the top of the canister; TROM [run-of-mine temperature] numbers on thermocouple labels increase with distance from canister, with 5.08-cm [2-inch] spacing between measurements). Temperature stabilized after about 15 d (vertical dashed line), excluding a minor drop during a power outage. (B) Temperatures at the canister boundary and at the ends of thermocouple arrays after 90 d. Points mark locations of corresponding measurements within the pile; red lines indicate thermocouple arrays as in Fig. 1A.

where C_p is the specific heat of the water, T is temperature, P is pressure, V_l is the specific volume, g is the absolute magnitude of gravity, and z is the height above a reference in the direction away from the center of mass of the gravity field.

Thermal conductivity for non-salt portions of the model is specified by the user directly. Within the salt medium, thermal conductivity is a function of both temperature and porosity. The temperature dependence is based on Munson et al. (1990) as

$$\kappa_{T\text{-}WIPP}(T) = \kappa_{T\text{-}300}\left(\frac{300}{T}\right)^{1.14} \quad [15]$$

where T is temperature (K) and $\kappa_{T\text{-}300}$ is the thermal conductivity of pure halite at 300 K (5.4 W m^{-1} K^{-1}). Porosity n and thermal conductivity are related based on the function of Gable et al. (2009), which was developed as an equation fit to data from Bechtold et al. (2004) at the Asse salt mine in Germany. This function is the same as used in Eq. [2] above:

$$\kappa_{\text{T-ASSE}}(n) = -270n^4 + 370n^3 - 136n^2 + 1.5n + 5 \quad [16]$$

Above porosity values of $n \approx 0.4$, this function becomes unphysical. Consequently, we apply a linear decrease in thermal conductivity with increasing porosity, so that at $n = 1$ the thermal conductivity value is that of air. Temperature and porosity effects on thermal conductivity are combined by scaling $\kappa_{\text{T-ASSE}}$ to match $\kappa_{\text{T-300}}$ at $n = 0$:

$$\kappa_{\text{T-300}}(n) = \left[\frac{\kappa_{\text{T-300}}}{\kappa_{\text{T-ASSE}}(n=0)}\right]\kappa_{\text{T-ASSE}}(n) \quad [17]$$

In this case, $\kappa_{\text{T-300}}/\kappa_{\text{T-ASSE}}$ is 5.4/5.0 or 1.08.

The FEHM salt functions (Harp et al., 2014; Stauffer et al., 2015; Bourret et al., 2016; Johnson et al., 2018) include the solubility of salt in water with temperature as derived from Sparrow (2003). Porosity changes are based on the transition of salt between liquid and solid phases. Precipitation of salt reduces porosity, while dissolution increases porosity; thus, porosity is updated in each chemistry iteration *ic* as

$$\Delta n_{\text{ic}} = -\Delta c \rho_{\text{s}} M_{\text{s}} \frac{1}{\rho_{\text{NaCl}}}(1 - n_{\text{ic}}) \quad [18]$$

where Δc is the change in moles of solid salt per weight of the solid (kg), ρ_{s} is the density of the solid (kg m^{-3}), M_{s} is the molar mass of the solid (kg mol^{-1}), and ρ_{NaCl} is the density of salt, with $\rho_{\text{s}} = \rho_{\text{NaCl}}$. Permeability is related to porosity based on Cinar et al. (2006), constrained to lie between a maximum of 0.9999 and a minimum of 10^{-5}.

Water vapor diffusion accounts for thermal and pressure effects and is described by

$$D_{\text{va}} = \tau D_{\text{va}}^{\text{o}} \left(\frac{P_{\text{o}}}{P}\right)\left(\frac{T + T_{\text{o}}}{T_{\text{o}}}\right)^{1.81} \quad [19]$$

where τ is tortuosity, $D_{\text{va}}{}^{\text{o}} = 2.23 \times 10^{-5}$ m^2 s^{-1}, $T_{\text{o}} = 273.15$ K, T is temperature (°C), P is pressure (MPa), and $P_{\text{o}} = 0.1$ MPa (Pruess 1991). Water vapor pressure is a function of temperature and is lowered by the presence of salt and other additional materials in the WIPP setting (Bourret et al., 2016, 2017). The effective free-air water vapor diffusion coefficient is then modified based on the Millington and Quirk (1961) relationship. A modified tortuosity term for gas transport in porous media is applied (Ho and Webb, 1998; Stauffer et al., 2009):

$$\tau = \frac{(S_{\text{a}} n)^{7/3}}{n^2} \quad [20]$$

Diffusive mass transport of water vapor through air is

$$\mathbf{f}_{\text{mwv}} = -D_{\text{va}} n S_{\text{v}} W_{\text{Mwv}} \nabla C_{\text{wv}} \quad [21]$$

where $\mathbf{f}_{\text{mwv}}$ is the diffusive mass flux of water vapor, W_{Mwv} is the molecular weight of water vapor (kg mol^{-1}), and C_{wv} is the moles of water vapor per cubic meter. Non-condensable gas (air) is allowed to diffuse along its concentration gradient with a diffusive mass flux as

$$\mathbf{f}_{\text{ma}} = -D_{\text{va}} n S_{\text{v}} W_{\text{Mwa}} \nabla C_{\text{a}} \quad [22]$$

where $\mathbf{f}_{\text{mwa}}$ is the diffusive mass flux of air, W_{Ma} is the molecular weight of air (kg mol^{-1}), and C_{wa} is the moles of air per cubic meter.

Porosity effects are expressed using a porosity change severity index, ψ. This index is calculated as the sum of the magnitude of the porosity change at each *i*th node:

$$\Delta V = \sum_{i=1}^{\alpha} |\text{dn}_i| V_i \quad [23]$$

where α is the total number of nodes in the RoM salt pile, dn_i is the porosity change at a given node, and V_i is the volume represented by the node. The ratio of ΔV to the total pile volume V_{t} yields the index of the severity of porosity changes, ψ, as

$$\psi = \frac{\Delta V}{V_{\text{t}}} \quad [24]$$

Capillary effects in the RoM salt pile are simulated using a dynamic, porosity-dependent retention function (Johnson et al., 2017b, 2018). The function changes residual saturation and maximum capillary pressure at each time step based on updated porosity, thereby strengthening capillary forces in nodes where porosity decreases and weakening them where porosity increases and pore diameters expand. Saturation-only retention functions can lead to unphysical results when porosity greatly increases, such as capillary pressure causing water to be retained in nodes where no actual porous medium remains. Accounting for porosity in the retention function prevents such issues.

Simulation Domain, Boundary Conditions, and Approach

Based on characterization of the experiment within WIPP, a thin (0.2-m) computational mesh (nominally two dimensional) was developed (Fig. 4B), representing an east–west slice through the center of the canister. We adopt a Cartesian reference frame with the positive *x* axis to the east, perpendicular to the long axis of the canister; the positive *y* axis to the north, parallel to the long axis of the canister; and gravitational acceleration in the $-z$ direction. Overall dimensions of the domain are 18.7-m width (*x* direction), 0.2-m length (*y* direction), and 36.6-m height (*z* direction). The canister center is at the origin and has a radius of 0.3048 m (1 ft). The bottom of the canister contacts the floor of the simulated drift at a single node. The RoM salt surrounds the canister as shown in the schematic (Fig. 4A). Air extends vertically above and laterally in the *x* direction (east) surrounding the pile. The DRZ surrounds the open air of the drift and forms the bottom ($-z$) and left ($-x$) boundaries of the salt pile. Damage in the DRZ is expressed as order-of-magnitude higher porosity and increased permeability following Jordan et al. (2015c).

A far-field rock boundary of constant 28°C and 10 MPa are assigned at the maximum $-z$, minimum $-z$, and minimum $-x$ (top, bottom, and left) edges of the intact salt unit. A constant air pressure of 0.101 MPa is assigned to a node in the air region along the positive $-x$ edge of the domain, slightly below the top of the

simulated open drift. This boundary adds or removes gas as necessary to maintain the specified air pressure. In tandem with the air input, an additional boundary condition is applied at the higher pressure air node, which specifies a fixed mixing ratio of air/water vapor, representing constant humidity. Water vapor mass is added or removed to maintain this specified mixing ratio at the boundary node. Based on the average annual temperature and humidity in WIPP (Bourret et al., 2017), this value is assigned as a constant 0.8906. This average ratio represents humid air and provides a conservative estimate for humid-air input of moisture to the pile. A corresponding node of constant 0.100-MPa gas pressure is placed at the top of the air zone directly above the pile, inducing a flow of the specified humidity air across the top of the RoM salt pile to simulate the flow of ventilation air in the experimental drift. This combination of boundary conditions drives air at a fixed humidity through the drift and across the top of the pile, adding or removing water from the RoM salt. The temperature above the pile was not continuously measured, but sampling after the pile attained steady state indicates that air within a few centimeters of the top of the pile remains within 0.01°C of ambient air elsewhere in the drift. Air in the simulations is therefore fixed to a constant 28°C.

For all scenarios presented, we begin with an isothermal background simulation to establish the initial condition of the pile emplacement, followed by a simulation with the heat source applied. Background simulations were typically run for 365 d of model time, except where otherwise described below. Finally, the full 100-d simulation with added heat was activated from the background condition. Simulations take between 2 and 48 h to complete, with greater porosity redistribution leading to longer simulation times. Here we describe a general range of results and simulation behaviors as parameters were varied. Reproducing more detailed experimental results with respect to porosity changes will be undertaken after excavation of the salt pile in late 2018.

Table 1. Base case simulation parameters. Highlighted values indicate parameters that are varied to improve model fit.

Property	RoM salt†	DRZ salt‡	Rock salt	Canister edge	Ceramic beads§
Porosity	0.3	0.01	0.001	10^{-5}	10^{-5}
Permeability, m^2	10^{-12}	10^{-17}	10^{-20}	10^{-22}	10^{-22}
Density¶, kg m^{-3}	2165.0	2165.0	2165.0	8000.0	1690.0
Thermal conductivity, W m^{-1} K^{-1}	1.03	5.2	5.4	15.0	0.24
Specific heat capacity¶, MJ kg^{-1} K^{-1}	931.0	931.0	931.0	500.0	100.0
Initial saturation	0.01	0.1	1	10^{-6}	10^{-6}
Maximum capillary pressure, MPa	0.5	1.0	1.0	0.0	0.0

† Run-of-mine salt.
‡ Damaged rock zone salt.
§ Properties of the ceramic beads inside the canister were fit to data from an earlier experiment (Jordan et al., 2015c).
¶ Note that density and specific heat capacity are specified for the solid matrix and modified within the model by porosity and saturation for bulk material properties.

Model Calibration Approach

Initial heating of the pile and the achievement of an approximate steady-state temperature in the experiment provide an opportunity to calibrate model simulations against the measured data. Matching the steady-state temperature in the simulations to the experiment allows estimation of thermal parameters and, to an extent, material properties within the crushed salt and the DRZ beneath the drift. Thus, we apply known material properties where possible to the model domain, such as those of stainless steel to the canister rim, thermal properties of cerabeads (Jordan et al., 2015c), and intact salt in the walls (Table 1). For the calibration presented below, two remaining free parameters, thermal conductivity of the DRZ and RoM salt, were varied manually to improve the match between simulated and measured temperatures. In addition, we also modified the thermal conductivity values of the nodes just beneath the simulated base of the canister and salt pile.

Sensitivity Simulation Approach

We conducted a set of four primary sensitivity analyses designed to explore simulated porosity changes in the RoM salt pile surrounding the heated canister during 100 d of heating.

Run-of-Mine Saturation Sensitivity

The sensitivity of the simulated porosity change with respect to RoM saturation is examined by varying the initial saturation of the RoM pile from 0.001 to 0.1 (Table 2). This range is constrained by the volume of water available within the mined salt and its subsequent mass changes. Assuming that dense rock salt (porosity = 0.001) is fully saturated, its volumetric water content (porosity × saturation) would be 0.001. If that salt was ground up and deposited in a pile with a porosity of 0.3, the saturation of the resulting RoM salt pile would be about 0.003, close to our minimum estimate of 0.001. A maximum estimate is more difficult to constrain but is likely to fall near the residual saturation of the material, which is unknown and probably variable. Prior experimental work (Olivella et al., 2011) determined a residual saturation value in fine granular salt of about 0.05. Allowing for some error from case to case, we estimate a maximum initial RoM saturation of 0.1. An evaporation pan experiment indicated that if the relative humidity of the ambient air surpassed about 28%, a small mass of water would enter the pile, while any lower relative humidity value would dry the pile (Bourret et al., 2017). WIPP RoM salt is probably fairly dry as a result of the general low humidity near the air

Table 2. Parameters for run-of-mine (RoM) saturation sensitivity studies.

Parameter	Value
RoM saturation	0.001, 0.01, 0.05, 0.1
DRZ† saturation	0.1
RoM maximum capillary strength‡, MPa	0.5
DRZ maximum capillary strength, MPa	1.0
Background run time, d	365

† DRZ, damaged rock zone.
‡ Value varies during the model run at each node; listed value is as initially specified.

intake over the course of years. How these results would translate to other rock salt compositions and other locations is unknown.

Damaged Rock Zone Saturation Sensitivity

The saturation of the DRZ is a major uncertainty and probably varies spatially at WIPP, depending on both geologic heterogeneity and the length of elapsed time between opening of the drift and emplacement of the radiogenic sources. We assume that the DRZ is initially fully saturated and gradually desiccates as moisture is entrained into air passing through the repository. An additional complication is the potential generation of brine from mineral hydration and the release of trapped brine from pores in the salt. Experiments to further examine these topics are in development (Johnson et al., 2017a). We consider a range from 0.05 (possible residual saturation) to 1.0 (fully saturated) for the initial DRZ saturation (Table 3).

Relative Capillary Strength Sensitivity

Saturation of the DRZ impacts flow toward the RoM pile in two ways. First, increased DRZ saturation increases the amount of water available to the RoM salt pile. Second, increased DRZ saturation reduces the initial capillary pressure of the DRZ, allowing capillary forces to draw moisture into the RoM salt. In addition, the capillary strength of the dry RoM salt pile itself is of crucial importance because it may draw brine to the canister to replace evaporated moisture. Strong capillary effects within the DRZ will tend to counteract those of the RoM salt, retaining water in the DRZ instead of allowing it to enter the RoM salt pile. We therefore conducted two suites of sensitivity simulations to illuminate the role of capillary forces between the DRZ and the RoM salt pile. In the first, the DRZ is initially at its low default saturation, and the maximum initial capillary pressure of the dry RoM salt pile is varied (Table 4). In the second, the DRZ is initially fully saturated and RoM capillary effects are varied. These simulations place boundaries on the effects of varying capillary action by examining both the case of competing capillary forces and the effects of varying the magnitude of capillary forces at early time in the saturated-DRZ case.

Time after Drift Opening

Following the opening of a drift, several different processes are expected to occur simultaneously. As noted in the DRZ saturation study discussed above, moisture in the DRZ will tend to be drawn into ambient air flowing through the facility. A low-pressure front will advance into the walls of the drift from the open air because the atmospheric pressure open air boundary is placed adjacent to fluids at hydrostatic or lithostatic pressure. We therefore selected a pressure of 10 MPa for the DRZ as the starting point for these simulations. A background run was conducted in which the salt pile and canister were simulated using the same properties assigned to air (Table 1). The duration of this run represents the elapsed time between opening of the drift and emplacement of the pile (Table 5). After the background run completed, a new simulation was conducted in which initial conditions were read from the output of the previous simulation, and salt pile and canister properties were applied. As specified, the DRZ attained a steady state at about 60 d, after which time little change in saturation or pressure occurred.

Table 3. Parameters for damaged rock zone (DRZ) saturation studies.

Parameter	Value
RoM† saturation	0.01
DRZ saturation	0.05, 0.1, 0.3, 0.5, 0.7, 1.0
RoM maximum capillary strength‡, MPa	0.5
DRZ maximum capillary strength, MPa	1.0
Background run time, d	365

† RoM, run-of-mine.
‡ Value varies during the model run at each node; listed value is as initially specified.

Table 4. Parameters for run-of-mine (RoM) and damaged rock zone (DRZ) capillary strength sensitivity studies.

Parameter	Value
RoM saturation	0.01
DRZ saturation	0.1 and 1.0
RoM maximum capillary strength†, MPa	0.05, 0.07, 0.1, 0.3, 0.5, 1.0
DRZ maximum capillary strength, MPa	1.0
Background run time, d	365

† Value varies during the model run at each node; listed value is as initially specified.

Simulation Results

Model Calibration: Simulations of a 15-Day Heating Period

Using the analytical estimate of 1 W m^{-1} K^{-1} for thermal conductivity of the pile and base case parameters from Table 1, we simulated 15 d of model time with constant material properties and compared the temperature of the node nearest the measurement points shown in Fig. 4B. Thermal conductivity of the DRZ and RoM units were varied manually to improve the temperature match, and final values of these parameters are listed in Table 1. For these initial heating runs, the porosity change components of the model were not active, and a fixed thermal conductivity value was used.

Table 5. Parameters for study of time after drift opening for run-of-mine (RoM) and damaged rock zone (DRZ).

Parameter	Value
RoM saturation	0.01
DRZ saturation†	1.0
DRZ liquid pressure†, MPa	10.0
RoM maximum capillary strength‡, MPa	0.5
DRZ maximum capillary strength, MPa	1.0
Background run time, d	0, 1, 3, 5, 7, 10, 15, 30, 45, 60, 75, 90, 100, 365

† Initial value.
‡ Value varies during the model run at each node; listed value is as initially specified.

This calibrated simulation yields a close match to measured data (within 5°C) on the sides of the canister and in the RoM salt pile on either side (x and $-x$ directions from the canister center). The initial heating rate above the canister is slightly higher in the simulations than in the experiment, although the two values converge after the first few days. Since the temperature divergence occurs from the beginning of the experiment and model time, and the thermocouple array does not show any long-term increases or decreases that would suggest changing thermal conductivity over time, the difference is unlikely to be produced by porosity changes from heat–brine interactions. Based on the overall close match of simulation and experiment temperature results, we elected to use the ~1 W m^{-1} K^{-1} thermal conductivity value for subsequent simulations.

Although the base-case simulations were able to capture the temperature in the RoM salt pile quite well, the temperature profile in the floor beneath the canister shows a sudden sharp drop between the base of the canister and the first thermocouple (Fig. 6) that was not seen in the base-case simulation. Furthermore, measured temperatures at the base of the canister are unexpectedly hot if we assume that the canister is in direct contact with intact, highly conductive salt (>5 W m^{-1} K^{-1}). We believe that the elevated temperatures seen directly beneath the canister in the active experiment are related to the placement of the experiment near the WIPP air intake shaft. Material from higher stratigraphic layers travels down the intake shaft and leaves a layer of fine material on the floor. This material is not composed of salt. Consequently, the coupling between the canister and underlying intact salt is relatively poor in the experiment. By allowing for slightly higher thermal conductivity within the pile and adding a thin insulating layer below the pile (about 2 cm), we were able to match temperatures beneath the pile to within 5°C (Fig. 7). However, for the subsequent parameter sensitivity analysis, we elected to assume direct contact between the canister and the DRZ in the floor of the drift, as would be expected in an active disposal setting where outside dust has not been permitted to accumulate over decades.

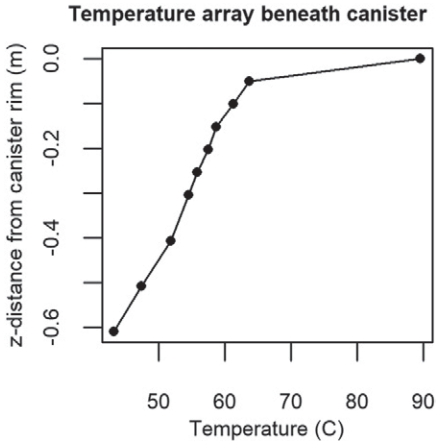

Fig. 6. Temperature profile in the small-diameter borehole beneath the heater canister.

Sensitivity Simulation Results

Although the specific locations and magnitudes of porosity change varied among simulations, overall trends can be identified. An increased ψ value generally relates to the formation of a band of dissolution and precipitation along the junction of the RoM salt and the DRZ (Fig. 8A–8C). In the simulations with the least porosity change (ψ < ~0.5), weak dissolution is localized within the RoM pile near the vertical wall of the DRZ where brine enters the pile, with an accompanying minor decrease in porosity nearer the canister where evaporation of brine causes salt to precipitate (Fig. 8A). As ψ increases, the base of the RoM pile between the canister and the wall begins showing a stronger dissolution effect (Fig. 8B). A slight decrease in porosity (<0.01) appears above the canister, and an outer dissolution band develops along the wall side of the pile. Directly beneath the canister, porosity drops to its minimum value due to the evaporation of brine and precipitation of salt (Fig. 8C). These same regions of porosity change increase in magnitude and spatial extent as ψ increases further.

Finally, we present parameter sensitivity results for investigations of the initial saturation of the RoM pile (Fig. 8D), saturation of the DRZ (Fig. 8E), the relative strength of the maximum capillary pressure in the RoM salt compared with the DRZ (Fig. 8F), and simulations in which the DRZ is allowed to dry and depressurize for varying lengths of time (Fig. 8G). Each plot shows the porosity change severity index ψ as a function of the relevant variable. The index ψ scales approximately linearly with the initial saturation of the RoM salt and causes the greatest changes within the RoM pile. However, porosity changes associated with increasing RoM saturation are primarily expressed as a general decrease throughout the pile due to the precipitation of salt as water evaporates out of saturated brine. Sensitivity of ψ to the saturation of the DRZ is less than to RoM saturation until a critical threshold, when it suddenly increases rapidly. For equally saturated RoM and DRZ salt, the relative maximum capillary strength of the RoM salt pile compared with the DRZ has little effect on ψ if capillary forces in the dry RoM pile are weak compared with the dry DRZ.

Based on the sensitivity to DRZ saturation, the elapsed time between opening of the drift and emplacement of the canister and ROM is likely to be important because the initially saturated walls of the DRZ dewater toward the drift while losing water to evaporation. Our final sensitivity analysis investigates this topic (Fig. 8G) by adjusting the time of the initial background simulations, allowing for evaporative drying of the drift walls. Background simulations stabilize to a steady-state condition at about 60 d, as a steady pressure gradient from the far field boundary to the atmospheric boundary is established. As shown in Fig. 8G, effects of DRZ drainage and depressurization on the pile rapidly decrease after the first few days.

Discussion and Conclusion

We examined the sensitivity of parameters (initial ROM saturation, DRZ saturation, RoM/DRZ capillary pressure ratio, and time between drift opening and waste placement) for their

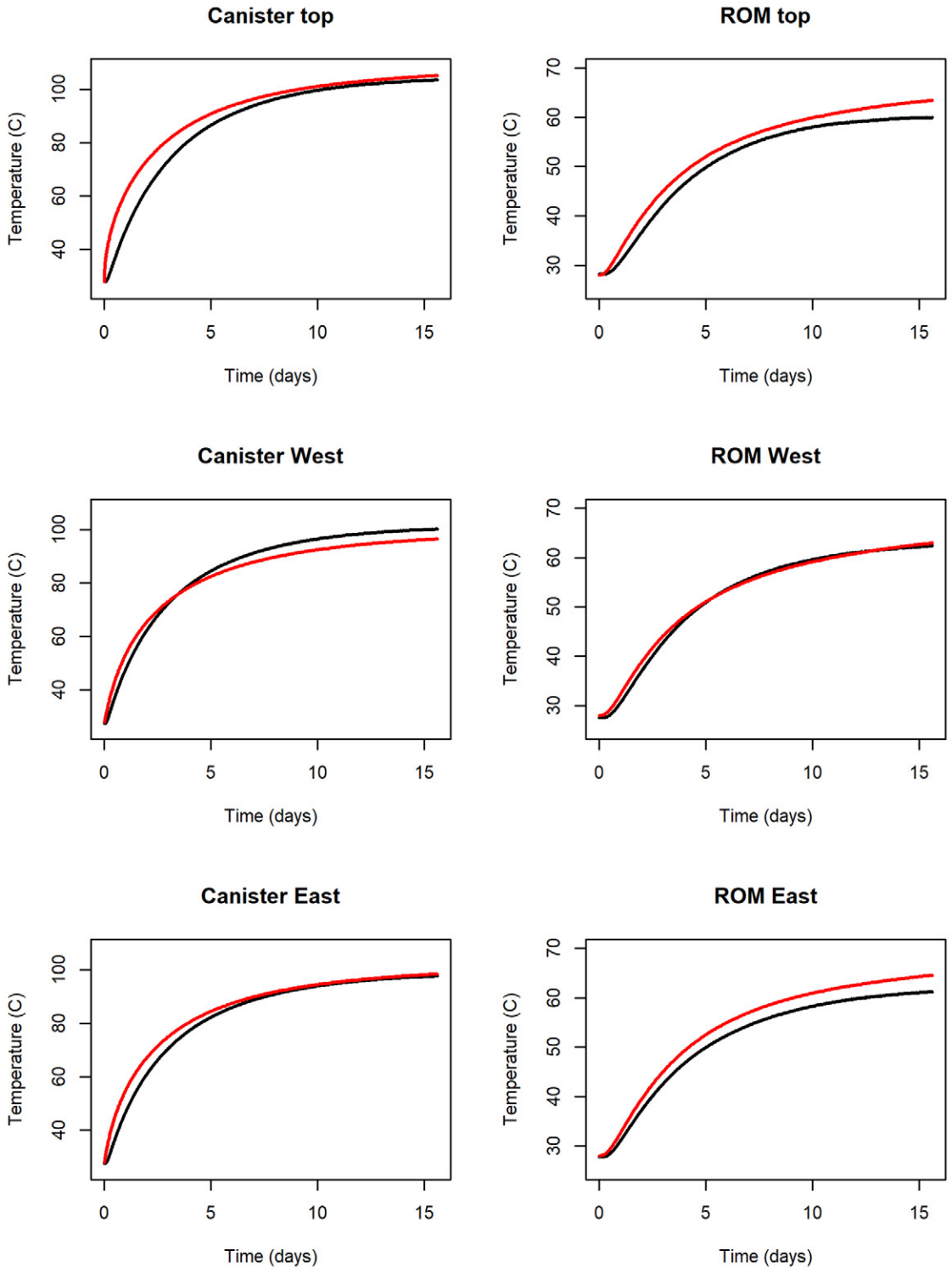

Fig. 7. Comparison of simulation results (red) with experimental results (black) for measurement points on the top and sides of the canister. Run-of-mine (RoM) results are for thermocouple measurements located 0.3048 m (1 ft) away from the canister in the salt pile, along the directions indicated.

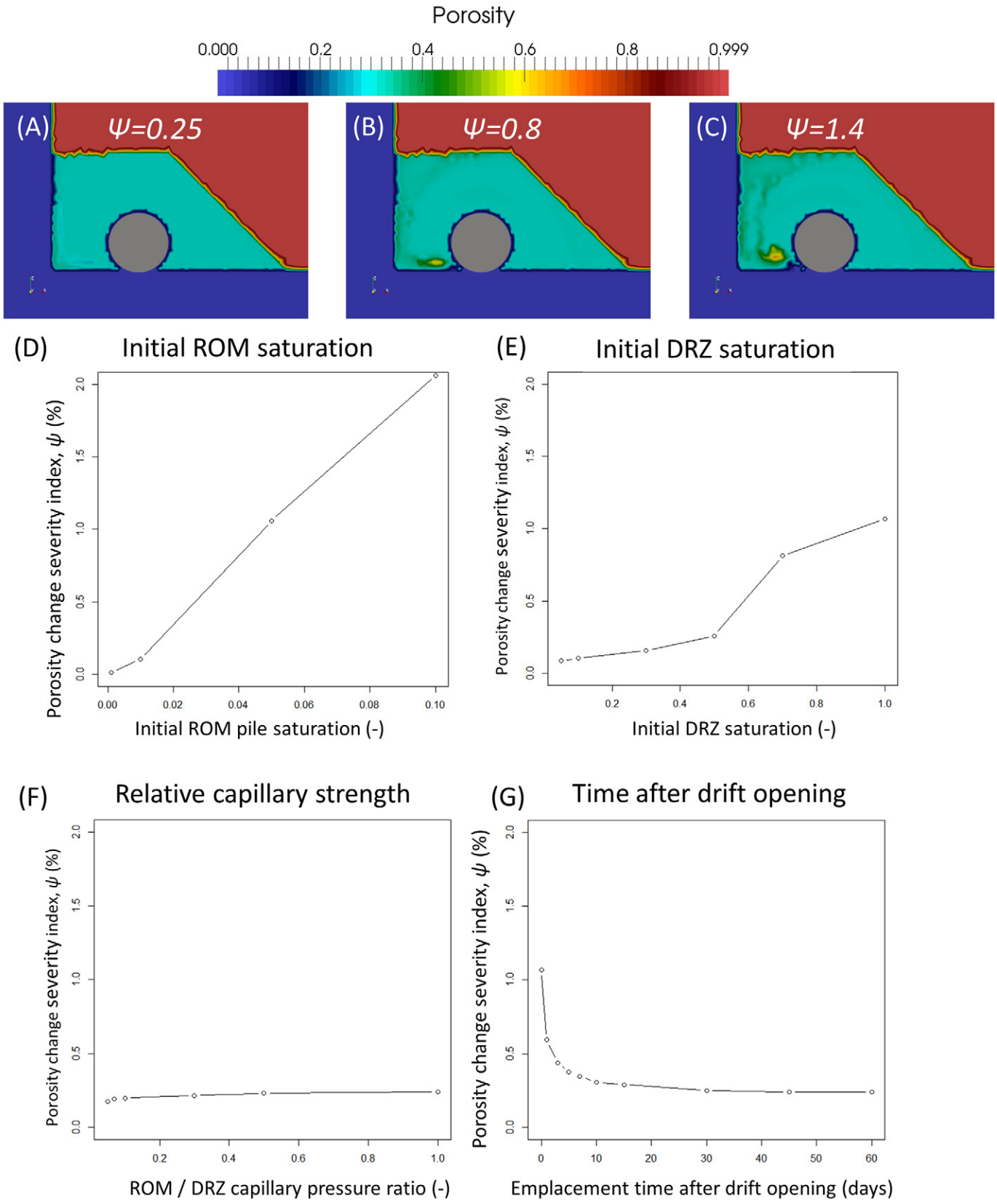

Fig. 8. Sum of absolute value of porosity changes in the run-of-mine (RoM) salt pile (Ψ) resulting from different parameters: (A,B,C) example porosity effects with increasing Ψ; (D) RoM saturation; (E) initial damaged rock zone (DRZ) saturation; (F) ratio of strength of maximum capillary effects in RoM salt vs. DRZ; and (G) elapsed time between opening of the drift and placement of the canister.

effect on the RoM salt pile dissolution and precipitation reactions. In contrast to previous work using retention functions that are not dependent on porosity, none of the simulations produced strong changes throughout the pile. Porosity changes are typically stronger near the wall of the drift and along the base of the RoM salt pile, where entry of brine from the surrounding rock occurs. The parameter of greatest sensitivity is the initial saturation of the RoM salt pile, which at a saturation of 0.1 produced about double the porosity change of the fully saturated DRZ, as calculated using the porosity change severity index (ψ). However, the 0.1 saturation value for RoM salt may be unrealistically high in a generic salt repository setting because it requires an additional brine source following mining of the salt; assuming fully saturated salt at a porosity of 0.01, the initial porosity of the resulting RoM salt at a porosity of 0.3 would be about 0.03. Additional brine might enter the RoM salt during the storage period between mining and emplacement of the canister from humid air or precipitation if RoM salt is stored outside, but the maximum reasonable value for these processes is unknown. Brine may also be generated in RoM salt by the dehydration of hydrous minerals during heating (Jordan et al., 2015a) or by the release of brine from fluid inclusions within the salt; however, no evidence of these processes was seen in this experiment.

Based on numerical simulations and experimental results during the first 100 d, little change is likely occurring in the RoM salt pile in the experiment. Temperature measurements indicate that thermal conductivity remains constant at a value typical for a porosity of 0.3, and no long-term trends are observed. If a strong dissolution band was forming, thermal conductivity would be expected to decrease and further raise temperature. Conversely, if a portion of the pile was decreasing in porosity, local thermal conductivity would increase toward the ~5.4 W m^{-1} K^{-1} typical of intact halite. Simulations showed that porosity effects over time tend to be stronger in the RoM pile between the heated canister and the wall of the gallery. If this effect was occurring within the pile, temperatures on the west (wall side) and east (drift side) of the pile would increasingly diverge over time, but this is not observed. The minor temperature variations after the initial heating period can probably be attributed to the cooling of ambient air due to the onset of winter, although a minor decrease in porosity and increase in thermal conductivity may account for the model overestimation of temperature in the top of the pile. It is possible that the top of the pile is slightly more compacted than the sides of the pile and consequently has a lower porosity and correspondingly higher thermal conductivity. Tamping down of the pile to produce the flattened top could have readily produced such a compaction increase.

In general, precipitation–dissolution appear to have little influence on the RoM pile in both the experiment and the simulations. Instead, a chimney effect and the flow of air through the drift combine to remove water vapor from the pile, reducing available brine and preventing recharge of brine toward the heat source. Relatively cool air from the drift enters the pile and heats, increasing its moisture holding capacity and desiccating the RoM salt. Warm, relatively dry air flows upward out of the pile and is entrained into the flow of ventilation air. The open chimney system causes a net drying of the RoM salt pile and restricts the cyclical dissolution–precipitation reactions that would be seen in a closed heat-pipe system (Olivella et al., 2011; Jordan et al., 2015c; Johnson et al., 2017b). Overall, this chimney effect is a contrast from prior experiments and simulations in closed systems, in which heat pipe effects produced strong porosity changes (Jordan et al., 2015b, 2015c; Johnson et al., 2017b; Olivella et al., 2011; Blanco-Martín et al., 2018). Additional changes within the RoM salt pile require a supply of brine, either from the DRZ or generated within the RoM salt pile by dehydration reactions.

Results for DRZ saturation and the ratio of maximum RoM to DRZ capillary pressure indicate that further porosity change can be induced in the pile by drawing water into the RoM salt pile from the wall and floor of the drift. However, this depends greatly on the quantity of water that is available in the DRZ. Since the DRZ capillary pressure at any given time depends on the saturation of the DRZ, there is a double sensitivity to DRZ saturation; increased DRZ saturation makes more brine available and also reduces the capillary strength of the DRZ and allows increased wicking of brine into the RoM salt pile. The break in the DRZ saturation curve (Fig. 8E) indicates the point at which DRZ saturation lowers the capillary pressure sufficiently to allow brine to enter the RoM salt pile.

Our work suggests several areas for further investigation. First, moisture content of RoM salt from different locations and in different climates may be important. For WIPP RoM salt, moisture content tends to increase when the relative humidity surpasses about 30% (Bourret et al., 2017). Furthermore, hydrous minerals within the RoM salt pile may dehydrate and contribute additional water (Jordan et al., 2015a). Minor fluid inclusions within individual salt clasts could also be released into the pile. Second, quantification of the brine available to the RoM pile from the surrounding walls needs to be improved. In addition to the initial porosity and permeability of the DRZ and intact wall rock, both of which can vary depending on local conditions, heating of the ambient salt drives reactions that release water. For typical WIPP salt, brine is released at temperatures between 60 and 90°C (Jordan et al., 2015a), slightly warmer than the in-progress experiment but potentially achievable with a higher wattage heat source and/or more canisters. With water liberated from hydrous minerals, additional brine could enter the RoM salt pile and amplify dissolution–precipitation effects around the heat source. Experiments are currently in development to further examine brine generation in response to heat in the drift walls at WIPP (Johnson et al., 2017a). Finally, our simulations show that stronger porosity changes are likely to occur in a fresh drift than in an older drift. The ongoing experiment could not be conducted in a fresh drift due to facility requirements at the time of construction, but subsequent experiments in a new drift could help provide evidence to validate conceptual and numerical models.

Acknowledgments

This work was completed through collaboration between USDOE-NE and USDOE-EM. Funding and resources to engineer, develop, shake down, and test a full-scale heater canister were initially provided in mid-FY 2013 through the USDOE Carlsbad Field Office to LANL-Carlsbad Operations. This activity encompasses the work to operationally test a finished prototype heater at various heat outputs under in situ conditions for use in future thermal tests in salt. As a collaborative effort, thermal and hydrological data collected for the operational test were used by Johnson to confirm model predictions, with funding for the numerical analysis provided by USDOE-NE through Grant DMS SFWD-SFWST-2017-000102.

References

Bechtold, W., E. Smailos, S. Heusermann, W. Bollingerfehr, B. Bzaragan Sabet, T. Rothfuchs, et al. 2004. Backfilling and sealing for underground repositories for radioactive waste in salt (BAMBUS II project). Final Rep. EUR 20621. Nuclear Science and Technology, Luxembourg.

Birkholzer, J.T. 2004. Estimating liquid fluxes in thermally perturbed fractured rock using measured temperature profiles. J. Hydrol. 327:496–515. doi:10.1016/j.jhydrol.2005.11.049

Blanco-Martín, L., J. Rutqvist, A. Battistelli, and J.T. Birkholzer. 2018. Coupled processes modeling in rock salt and crushed salt including halite solubility constraints: Application to disposal of heat-generating nuclear waste. Transp. Porous Media 124:159–182. doi:10.1007/s11242-018-1057-7

Bourret, S.M., P.J. Johnson, G.A. Zyvoloski, S.P. Chu, D.J. Weaver, S. Otto, et al. 2016. Experiments and modeling in support of generic salt repository science. USDOE Used Fuel Disposition Campaign, Final Rep. LA-UR-16-27329. Los Alamos Natl. Lab., Los Alamos, NM.

Bourret, S.M., S. Otto, P.J. Johnson, D.J. Weaver, H. Boukhalfa, and P.H. Stauffer. 2017. High level waste in salt repositories: Experiments and simulations of evaporation in the underground. In: 43rd Annual Waste Management Conference (WM2017): Education & Opportunity in Waste Management, Phoenix, AZ. 5–9 Mar. 2017. Vol. 6. Waste Manage. Symposia, Tempe, AZ. p. 3712–3722.

Brewitz, W., and T. Rothfuchs. 2007. Concepts and technologies for radioactive waste disposal in rock salt. Acta Montan. Slovaca 12(S1):67–74.

Callahan, G., D.C. Guerin, D.G. Levitt, D.L. Newell, B.A. Robinson, and L. Van Sambeek. 2012. Salt repository synthesis data of non-Delaware Basin and international programs for the storage/disposal of nuclear waste. Rep. LCO-SDI-002. Los Alamos Natl. Lab., Los Alamos, NM.

Caporuscio, F.A., H. Boukhalfa, M.C. Cheshire, A.B. Jordan, and M. Ding. 2013. Brine migration experimental studies for salt repositories. Milestone FCRD-UFD-2013-000204. Fuel Cycle Res. Dev., Used Fuel Disposition Campaign, Argonne Natl. Lab., Lemont, IL.

Carter, J.T., F. Hansen, R. Kehrman, and T. Hayes. 2011. A generic salt repository for disposal of waste from a spent nuclear fuel recycle facility. SRNL-RP-2011-00149 Rev. 0. Savannah River Natl. Lab., Jackson, SC.

Cinar, Y., G. Pusch, and V. Reitenbach. 2006. Petrophysical and capillary properties of compacted salt. Transp. Porous Media 64:199–228. doi:10.1007/s11242-005-2848-1

Faghri, A. 1995. Heat pipe science and technology. Taylor and Francis, Boca Raton, FL.

Fahland, S., and S. Heusermann. 2013. Geomechanical analysis of the integrity of waste disposal areas in the Morsleben repository. In: X.T. Feng et al., editors, Rock characterisation, modelling, and engineering design methods. CRC Press, Boca Raton, FL. p. 345–350.

Gable, C.W., D.J. Clayton, and Z. Lu. 2009. Inverse modeling to determine thermal properties of salt due to heating from high level waste emplaced in a generic salt repository. Rep. AFCI-WAST-PMO-DV-2009-000001. USDOE Office of Nuclear Fuel Recycling, Washington, DC.

Haar, L., J.S. Gallagher, and G.S. Kell. 1984. NBS/NRC steam tables. Hemisphere, New York.

Hansen, F.D., and C.D. Leigh. 2011. Salt disposal of heat-generating nuclear waste. Rep. SAND2011-0161. Sandia Natl. Lab., Albuquerque, NM.

Hansen, F.D.M., W. Steininger, and W. Bollingerfehr. 2017. Proceedings of the 7th US/German Workshop on Salt Repository Research, Design, and Operation. SFWD-SFWST-2017-000008, SAND2017-1057R. Sandia Natl. Lab., Albuquerque, NM.

Harp, D.R., P.H. Stauffer, P.K. Mishra, D.G. Levitt, and B.A. Robinson. 2014. Modeling of high-level nuclear waste disposal in a salt repository. Nucl. Technol. 187:294–307. doi:10.13182/NT13-110

Hess, H.H., J.N. Adkins, W.B. Heroy, W.E. Benson, M.K. Hubbert, J.C. Frye, et al. 1957. The disposal of radioactive waste on land. Publ. 519. Natl. Acad. Press, Washington, DC. doi:10.17226/10294

Ho, C., and S. Webb. 1998. Review of porous media enhanced vapor-phase diffusion mechanisms, models, and data: Does enhanced vapor-phase diffusion exist? J. Porous Media 1:71–92. doi:10.1615/JPorMedia.v1.i1.60

Johnson, P.J., H. Boukhalfa, D.J. Weaver, S. Otto, B.L. Dozier, P.H. Stauffer, et al. 2017a. Test plan document for thermal testing in salt. Milestone M3SF-18LA010303013, LA-UR-17-30762. Los Alamos Natl. Lab., Los Alamos, NM.

Johnson, P.J., S.M. Bourret, H. Boukhalfa, F.A. Caporuscio, G.A. Zyvoloski, D.J. Weaver, et al. 2017b. Experiments and modeling to support field test design. SFWD-SFWST-2017-000102, LA-UR-17-27759. Los Alamos Natl. Lab., Los Alamos, NM. doi:10.2172/1394993

Johnson, P.J., G.A. Zyvoloski, and P.H. Stauffer. 2018. Impact of a porosity-dependent retention function on simulations of porous flow. Transp. Porous Media (in press). doi:10.1007/s11242-018-1188-x

Jordan, A.B., H. Boukhalfa, F.A. Caporuscio, B.A. Robinson, and P.H. Stauffer. 2015a. Hydrous mineral dehydration around heat-generating nuclear waste in bedded salt formations. Environ. Sci. Technol. 49:6783–6790. doi:10.1021/acs.est.5b01002

Jordan, A.B., H. Boukhalfa, F.A. Caporuscio, and P.H. Stauffer. 2015b. Brine transport experiments in run-of-mine salt. Rep. LA-UR-15-26804. Los Alamos Natl. Lab., Los Alamos, NM.

Jordan, A.B., G.A. Zyvoloski, D.J. Weaver, S. Otto, and P.H. Stauffer. 2015c. Coupled thermal–hydrologic–chemical model for in-drift disposal test. Rep. LA-UR-15-27442. Los Alamos Natl. Lab., Los Alamos, NM.

Krieg, R.D. 1984. Reference stratigraphy and rock properties for the Waste Isolation Pilot Plant (WIPP) project. Report SAND-83-1908. Sandia Natl. Lab., Albuquerque, NM.

Kuhlman, K.L., and B. Malama. 2013. Brine flow in heated geologic salt. Rep. SAND2013-1944. Sandia Natl. Lab., Albuquerque, NM.

Lappin, A.R. 1988. Summary of site-characterization studies conducted from 1983 through 1987 at the Waste Isolation Pilot Plant (WIPP) site, southeastern New Mexico. In: R.G. Post, editor, Waste Management: Symposium on Radioactive Waste Management, Tucson, AZ. 28 Feb.–3 Mar. 1988. Vol. II: High-level waste and general interest. Nuclear Eng. Dep., Univ. of Arizona, Tucson. p. 371–376.

McTigue, D.F., and E.J. Nowak. 1987. Brine transport studies in the bedded salt of the Waste Isolation Pilot Plant (WIPP). Rep. SAND-87-1274C. Sandia National Lab., Albuquerque, NM.

Millington, R.J., and J.P. Quirk. 1961. Permeability of porous solids. Trans. Faraday Soc. 57:1200–1207. doi:10.1039/tf9615701200

Munson, D.E., R.L. Jones, J.R. Ball, R.M. Clancy, D.L. Hoag, and S.V. Petney. 1990. Overtest for simulated defense high-level waste (Room B): In situ data report (May 1984-February 1988), Waste Isolation Pilot Plant (WIPP) thermal/structural interactions program. Tech. Rep. SAND-89-2671. Sandia Natl. Lab., Albuquerque, NM.

Olivella, S., S. Castagna, E.E. Alonso, and A. Lloret. 2011. Porosity variations in saline media induced by temperature gradients: Experimental evidences and modeling. Transp. Porous Media 90:763–777. doi:10.1007/s11242-011-9814-x

Powers, D.W., S.J. Lambert, S.-E. Shaffer, L.R. Hill, and W.D. Weart, editors. 1978. Geological characterization report, Waste Isolation Pilot Plant (WIPP) site, southeastern New Mexico. Waste Manage. Technol., Sandia Natl. Lab., Albuquerque, NM.

Pruess, K. 1991. TOUGH2: A general-purpose numerical simulator for multiphase fluid and heat flow. Rep. LBL-29400. Lawrence Berkeley Natl. Lab., Berkeley, CA.

Rechard, R.P. 2000. Historical background on performance assessment for the Waste Isolation Pilot Plant. Reliab. Eng. Syst. Saf. 69:5–46. doi:10.1016/S0951-8320(00)00023-5

Robinson, B.A., N.Z. Elkins, and J.T. Carter. 2012. Development of a U.S. nuclear waste repository research program in salt. Nucl. Technol. 180:122–138. doi:10.13182/NT12-A14524

Rutqvist, J., L.B. Martin, S. Molins, D. Trebotich, and J. Birkholzer. 2016. Modeling coupled THM processes and brine migration in salt at high temperatures. UFD Doc. FCRD-UFD-2015-000366, LBNL-191216. Lawrence Berkeley Natl. Lab., Berkeley, CA.

Sparrow, B.S. 2003. Empirical equations for the thermodynamic properties of aqueous sodium chloride. Desalination 159:161–170. doi:10.1016/S0011-9164(03)90068-3

Stauffer, P.H., J.A. Vrught, H.J. Turin, C.W. Gable, and W.E. Soll. 2009. Untangling diffusion from advection in unsaturated porous media: Experimental data, modeling, and parameter uncertainty. Vadose Zone J. 8:510–522. doi:10.2136/vzj2008.0055

Stauffer, P.H., D.R. Harp, A.B. Jordan, Z. Lu, S. Kelkar, Q. Kang, et al. 2013. Coupled model for heat and water transport in a high level waste repository in salt. Doc. LA-UR-13-27584. Los Alamos Natl. Lab., Los Alamos, NM.

Stauffer, P.H., K.C. Lewis, J.S. Stein, B.J. Travis, P. Lichtner, and G.A. Zyvoloski. 2014. Joule-Thomson effects on the flow of liquid water. Transp. Porous Media 105:471–485. doi:10.1007/s11242-014-0379-3

Stauffer, P.H., A.B. Jordan, D.J. Weaver, F.A. Caporuscio, J.A. Ten Cate, H. Boukhalfa, et al. 2015. Test proposal document for phased field testing in salt. US DOE-NE Used Fuel Disposition Campaign, Level 2 Milestone M2FT-15LA08119016, FCRD-UFD-2015-000077. Doc. LA-UR-15-23154. Los Alamos Natl. Lab., Los Alamos, NM.

Tsang, C.F., F. Bernier, and C. Davies. 2005. Geohydromechanical processes in the excavation damage zone in crystalline rock, rock salt, and indurated plastic clays—in the context of radioactive waste disposal. Int. J. Rock Mech. Min. Sci. 42:109–125. doi:10.1016/j.ijrmms.2004.08.003

USDOE Carlsbad Field Office. 2012. A management proposal for Salt Defense Disposal Investigations (SDDI) for the disposal of DOE-EM managed wastes. USDOE Carlsbad Field Office, Carlsbad, NM.

Washington Savannah River Company, Washington Safety Management Solutions, Sandia National Laboratories, and Los Alamos National Laboratory. 2008. A generic salt repository for disposal of waste from a spent nuclear fuel recycling facility. Predecisional Draft, Rev 1 (September). GNEP-WASTMTSD-MI-RT-2008-000245. USDOE, Aiken, SC.

Weaver, D.J. 2014. Independent design analysis and verification of "heater canister" as part of the salt defense disposal investigation: Comprehensive final report. Rep. LA-UR-18-31862. Los Alamos Natl. Lab., Los Alamos, NM.

Wollrath, J., R. Mauke, M. Mohlfeld, M. Niemeyer, and D.A. Becker. 2014. Morsleben Repository: Interdependence of technical feasibility and functionality of geotechnical barriers and safety case development. Rep. NEA/RWM/R(2013)9. Radioactive Waste Management Committee, Nuclear Energy Agency of the OECD, Issy-les-Moulineaux, France.

Zyvoloski, G.A., B.A. Robinson, Z.V. Dash, S. Kelkar, H.S. Viswanathan, R.J. Pawar, et al. 2012. Software users manual (UM) for the FEHM Application Version 3.1-3.X. LANL Rep. LA-UR-12-24493. Los Alamos Natl. Lab., Los Alamos, NM.